Site-Specific Thermodynamics and Kinetics of a Coiled-Coil Transition by Spin Inversion Transfer NMR

D. André d'Avignon, G. Larry Bretthorst, Marilyn Emerson Holtzer, and Alfred Holtzer
Department of Chemistry, Washington University, St. Louis, Missouri 63130 USA

ABSTRACT A 33-residue pseudo-wild-type GCN4 leucine zipper peptide is used to probe the equilibrium conformational population in proteins. $^{13}C^{\alpha}$-NMR shows that chain sites differ in structural content at a given temperature, and that two dimeric *folded* forms are evident at many sites. Spin inversion transfer experiments are reported bearing on the thermodynamics and kinetics of interconversion of the two dimeric folded forms ($F_a \rightleftarrows F_b$) at the $^{13}C^{\alpha}$-labeled position L13. At each temperature, at conditions wherein the population of unfolded chains is quite small, inversion of the F_a spins via a tuned Gaussian π-pulse is followed by a time interval (τ), interrogation, and recording of the free induction decay. Fifteen such inversions, with varying τ, provide the time course for recovery of equilibrium magnetization after inversion. Similar experiments follow inversion of the F_b spins. Re-equilibration is known to be modulated by four first-order rate constants: two (T_{1a}^{-1} and T_{1b}^{-1}) for spin-lattice relaxation intrinsic to the respective sites, and two (k_{ab} and k_{ba}) for the conformational change. All four follow from joint, Bayesian analysis of all the data at each temperature. The equilibrium constant at each temperature for this local transition, determined simply from the equilibrium relative magnetizations at F_a and F_b sites, agrees well with the kinetic ratio k_{ab}/k_{ba}. The standard Gibbs energies, enthalpy, and entropy follow. Activation parameters, both ways, are accessible from the rate constants and suggest a transition state with high Gibbs energy and enthalpy, but with entropy *between* those of F_a and F_b.

INTRODUCTION

Information on the population of conformational states at equilibrium and on the kinetics of their interconversion is needed to gain a physical understanding of protein folding. One approach to the problem exploits experimental techniques that are site-specific. For example, such methods provide a direct test of the two-state model. If only native and unfolded molecular species coexist at equilibrium, then essentially all sites would show the same fraction folded at any temperature. If not, then local unfolding curves provide clues as to which conformationally intermediate states are present.

In this endeavor, proteins and peptides that form two-stranded coiled coils (Lupas, 1996; Privalov, 1982) have played an important role. The topological simplicity of the structure—two parallel, registered α-helices with a slight supertwist—provides a linear geometric context for the stabilizing interactions that is relatively transparent (McLachlan and Stewart, 1975). Indeed, statistical-mechanical theories have been developed, analogous to the Zimm-Bragg theory for single-chain helices, that describe the conformational complexity in some detail (Holtzer et al., 1990). Moreover, the link between the structure and the amino-acid sequence is reasonably clear: the sequence is characterized by a pseudo-repeating heptad (designated *abcdefg*), in which residues *a* and *d* are hydrophobic and *e* and *g* oppositely charged (McLachlan and Stewart, 1975).

Among the most-studied coiled coils is the leucine zipper (a coiled coil in which the *d* residues are leucines) from the GCN4 transcription factor (O'Shea et al., 1989, 1991). A study of hydrogen exchange in this peptide showed site-dependent protection factors, pointing to markedly different dynamics even at neighboring sites (Goodman and Kim, 1991).

Recently, a pseudo-wild-type GCN4 leucine zipper has been studied extensively by ultracentrifugation, CD, and $^{13}C^{\alpha}$-NMR (Lovett et al., 1996; Holtzer et al., 1997). This variant peptide (called here GCN4-lzK) differs from the native GCN4 leucine zipper by four conservative mutations: R1K, H18K, R25K, and R33K. Its full sequence appears in the following paragraph. GCN4-lzK forms a stable two-chain coiled coil, which undergoes the concentration-dependent thermal unfolding typical of coiled coils. A series of isosequential GCN4-lzK peptides, each labeled with 99% $^{13}C^{\alpha}$ at sites chosen to avoid NMR spectral overlap, provides several insights into the population of coexisting conformational states: 1) separate resonances are seen for folded and unfolded species at a given site, making it possible to obtain site-specific thermal unfolding curves; 2) the observed local unfolding transitions differ from site to site; 3) at most (but not all) sites, separate resonances are seen for more than one folded form.

These results clearly indicate that a rather rich array of conformational states coexist at thermal equilibrium. Here, we present data showing that more detailed information on these local transitions, including kinetic as well as thermodynamic constants, can be obtained from spin-inversion transfer (SIT) NMR. Specifically, we employ in this study

Received for publication 5 January 1998 and in final form 24 February 1998.

Address reprint requests to Alfred Holtzer, Department of Chemistry, Washington University Campus Box 1134, One Brookings Drive, St. Louis, MO 63130-4899. Tel.: 314-935-6572; Fax: 314-935-4481; E-mail: holtzer@wuchem.wustl.edu.

© 1998 by the Biophysical Society

0006-3495/98/06/3190/08 $2.00

the GCN4-lzK sequence: Ac-KMKQLEDKVEEL*L*SKN-YKLENEVAKLKKLVGEK-Am, wherein the underlined residues, L13(*e*) and G31(*b*), each bear a 99% $^{13}C^{\alpha}$ label.

In particular, we report studies on the interconversion of the two folded forms at chain position L13(*e*). The reaction may be written: $F_a \rightleftarrows F_b$, wherein F_a is the local folded form that dominates at the lowest temperatures and F_b is the local folded form that dominates at intermediate temperatures. Thermodynamic data (equilibrium constants) as a function of temperature are obtained from experimental spin counts of the two folded forms at conformational and spin equilibrium in the applied magnetic field. Rate constants for the forward (k_{ab}) and reverse (k_{ba}) reactions are obtained from the SIT experiments. These studies are carried out at a peptide concentration and in a range of temperatures such that the population of unfolded forms is quite small (Lovett et al., 1996; Holtzer et al., 1997).

In the SIT experiment, the solution is first equilibrated at the desired temperature in the applied magnetic field and its Fourier-transform $^{13}C^{\alpha}$-NMR spectrum determined. Then, a Gaussian π-pulse, tuned to the frequency of one of the locally folded species at L13(*e*), is applied, inverting, say, the F_b magnetization. The return of the magnetization to equilibrium at both sites is modulated by four rate constants: the intrinsic spin-lattice relaxation constants at the respective sites, T_{1a}^{-1} and T_{1b}^{-1}; and the forward and reverse conformational interconversion rate constants, k_{ab} and k_{ba}. Spectra taken at various times after inversion characterize the overall recovery at each site. Subsequent inversion at the F_a sites then provides an analogous data set. The differential equations governing the process, and their solutions, are long-known (McConnell, 1958; Rudin and Sauter, 1992); and joint analysis, via Bayesian probability theory, of the two sets of data provides values of all four rate constants for a given temperature.

The reader should bear two features of these experiments in mind. First, during the entire SIT experiment, the system is at conformational equilibrium; only the orientation of the nuclear spins is affected by the inversion. Kinetic constants for the conformational interconversion are therefore determinable even though the mobile conformational equilibrium is never disturbed. Second, the kinetic and thermodynamic properties determined refer to a transition converting the ensemble of chains in folded form F_a at residue L13(*e*) to the ensemble of chains in folded form F_b at that site. As will be seen, some conclusions concerning the nature of the overall transition and of the transition state for the process are suggested by the results.

MATERIALS AND METHODS

Synthesis, purification, and characterization of GCN4-lzK labeled at L13(*e*) and G31(*b*)

The solid-phase synthetic methods; procedures for preparing the $^{13}C^{\alpha}$-labeled Fmoc-amino acids and incorporating them into the growing peptide chain; and methods for purifying and characterizing the completed, end-capped peptide, have been described earlier (Holtzer et al., 1995, 1997; Lovett et al., 1996).

The molar mass of the purified peptide was found to be 3946.7 Da (3946.5 Da, expected) from electrospray mass spectrometry. The purified peptide is >98% pure by reversed-phase high-performance liquid chromatography using a Vydac C18 column (4.6 × 250 mm, 5 μ, 300-Å pore) with a 30–60% (v/v) acetonitrile gradient in 0.1% (v/v) trifluoroacetic acid at 1.5%/min. The thermal CD unfolding profile of the GCN4-lzK peptide, with 99% $^{13}C^{\alpha}$ at positions L13(*e*) and G31(*b*), is indistinguishable from that for the natural abundance peptide (Lovett et al., 1996). Peptide concentrations were determined from the absorbance of the solution at 275 nm with an extinction coefficient of 1.40 cm^{-1} M^{-1} for Y17 in benign, near-neutral, saline buffer.

$^{13}C^{\alpha}$-NMR

The equilibrium and SIT experiments were carried out using solutions of the peptide chains at a formal concentration of 1.95 mM in $(NaCl)_{100}(NaPi)_{50}(D_2O)_{5514}(7.4)$, wherein we designate complex aqueous solvent media by giving the formula of each solute species with its millimolarity as subscript followed by the pH in parentheses. This millimolarity of D_2O corresponds to 10% (v/v). The unfolding equilibria of these GCN4-lzK peptides are independent of the presence of D_2O up to 17% (Lovett et al., 1996; Holtzer et al., 1997). Reversed-phase HPLC of solutions of the peptide before and after the SIT studies showed no differences in retention times or purity.

A few preliminary experiments at other concentrations in the relevant room temperature region showed little difference in the relative equilibrium population of folded forms. At the relatively high concentration of the SIT experiments, the population of unfolded (monomeric) forms is small in the relevant temperature range (Lovett et al., 1996; Holtzer et al., 1997).

All NMR data were collected at a nominal field strength of 11.75 tesla employing a Unity-Plus 500 Spectrometer (Varian Associates, Palo Alto, CA) equipped with a 10-mm probe (Nalorac Corp., Martinez, CA). The peptide solution was placed in a 10-mm NMR tube employing susceptibility plugs (Shigemi, Allison Park, PA). Optimum signal-to-noise was obtained with a vertical sample height of ~1.7 mm (~1.1 cm^3). A field-frequency ^2H lock was maintained throughout. Chemical shifts are referenced to external 2,2-dimethyl-2-silapentane-5-sulfonic acid (DSS), as in prior work (Holtzer et al., 1997). Sample temperature was calibrated and controlled to 0.1°C as previously described (Lovett et al., 1996; Holtzer et al., 1997). ^{13}C-NMR data with broadband GARP decoupling were taken over a spectral width of 12,686 Hz with relaxation delays of 2.1 s between transients.

Magnetization transfer data were generated by successively 1) issuing a Gaussian π-pulse of 30 ms duration, with 11.73 ms full width at half height, and centered at the resonance frequency of $^{13}C^{\alpha}$ at position L13(*e*) of GCN4-lzK in its F_b folded form (the downfield, i.e., less shielded, resonance); 2) delaying by a variable interval (τ = 0–1.5 s); 3) interrogating via a 17.5 μs, broadband $\pi/2$ pulse; 4) recording the free induction decay (FID). Corresponding inversion at the F_a frequency (the upfield, i.e., more shielded, resonance) followed, with identical protocol. Approximately 1300 transients were recorded, with interleaving, among 15 separate delay times. Thus, at each temperature, 15 separate F_a and F_b magnetizations were measured following F_b inversion and an additional 15 F_a and F_b magnetizations following F_a inversion. The total collection time at each temperature is ~25 h.

Identical SIT protocols were used at a total of five temperatures in the range 21.1–32.6°C. An additional, equilibrium ^{13}C-NMR spectrum was recorded at each temperature with no signal inversion, using relaxation delays of 2.65 s between transients.

Bayesian data analysis

In the SIT experiment, the time course of the return to equilibrium is modulated by four rate constants: the respective spin-lattice constants at F_a

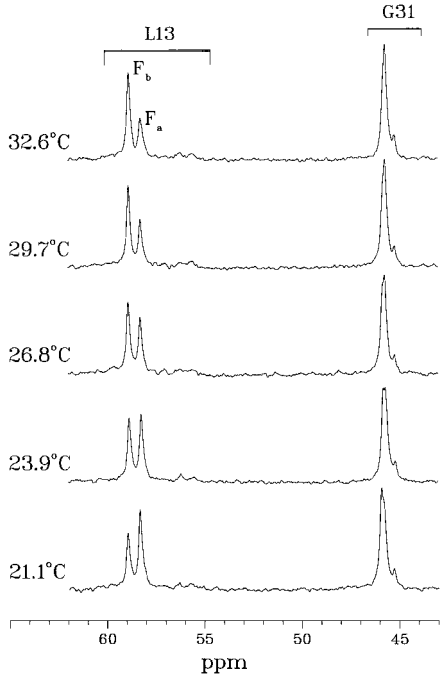

FIGURE 1 $^{13}C^{\alpha}$-NMR spectra of GCN4-lzK in $(NaCl)_{100}(NaPi)_{50}(D_2O)_{5514}$(7.4) near room temperature. Formal concentration of Peptide chains is 1.95 mM. Regions for full range of resonances at the respective labeled sites L13(*e*) and G31(*b*) are marked. L13(*e*) resonances assigned to local folded form favored at low T (F_a) and at moderate T (F_b) are also marked.

and F_b (T_{1a}^{-1} and T_{1b}^{-1}) and those for the forward (k_{ab}) and reverse (k_{ba}) conformational reactions $F_a \rightleftarrows F_b$. The modified Bloch differential equations appropriate to such a system and their solutions have long been known (McConnell, 1958; Rudin and Sauter, 1992). The coupled, first-order, inhomogeneous rate equations are most compactly presented in matrix form (Rudin and Sauter, 1992):

$$\frac{d}{dt}(\delta \mathbf{M}_{Zi}) = \mathbf{Y}\ \delta \mathbf{M}_{Zi} \tag{1}$$

where $\delta\mathbf{M}_{Zi}$ is the vector whose components give the deviation of the longitudinal (Z-direction) magnetic intensity at site i (M_{Zi}) from the equilibrium value at that same site (M_{Zi}^{eq}):

$$\delta \mathbf{M}_{Zi} = \begin{pmatrix} M_{Za} - M_{Za}^{eq} \\ M_{Zb} - M_{Zb}^{eq} \end{pmatrix} \tag{2}$$

and $\mathbf{Y}$ is the kinetic matrix:

$$\mathbf{Y} = \begin{pmatrix} -R_a & k_{ba} \\ k_{ab} & -R_b \end{pmatrix} \tag{3}$$

where $R_i = k_{ij} + T_{1i}^{-1}$.

The solution to Eq. 1 is

$$\delta \mathbf{M}_{Zi}(t) = \mathbf{U}^{-1}\begin{pmatrix} e^{a_1 t} & 0 \\ 0 & e^{a_2 t} \end{pmatrix}\mathbf{U}\ \delta \mathbf{M}_{Zi}(0) \tag{4}$$

where $a_{1,2}$ are the eigenvalues of the kinetic matrix $\mathbf{Y}$, and $\mathbf{U}$ and $\mathbf{U}^{-1}$ are reciprocal matrices suitable for similarity transformation of $\mathbf{Y}$. That is:

$$\mathbf{U}\ \mathbf{Y}\ \mathbf{U}^{-1} = \begin{pmatrix} a_1 & 0 \\ 0 & a_2 \end{pmatrix} \tag{5}$$

That Eq. 4 is the solution to Eq. 1 can be verified by substitution. The eigenvalues are obtainable from the matrix elements of $\mathbf{Y}$ via

$$a_{1,2} = \frac{-(R_a + R_b)}{2} \pm \frac{[(R_a - R_b)^2 + 4k_{ab}k_{ba}]^{1/2}}{2} \tag{6}$$

Various choices for the transforming matrices are legitimate. For example

$$\mathbf{U} = \frac{1}{a_1 - a_2}\begin{pmatrix} -(R_a + a_2) & k_{ba} \\ R_a + a_1 & -k_{ba} \end{pmatrix} \tag{7a}$$

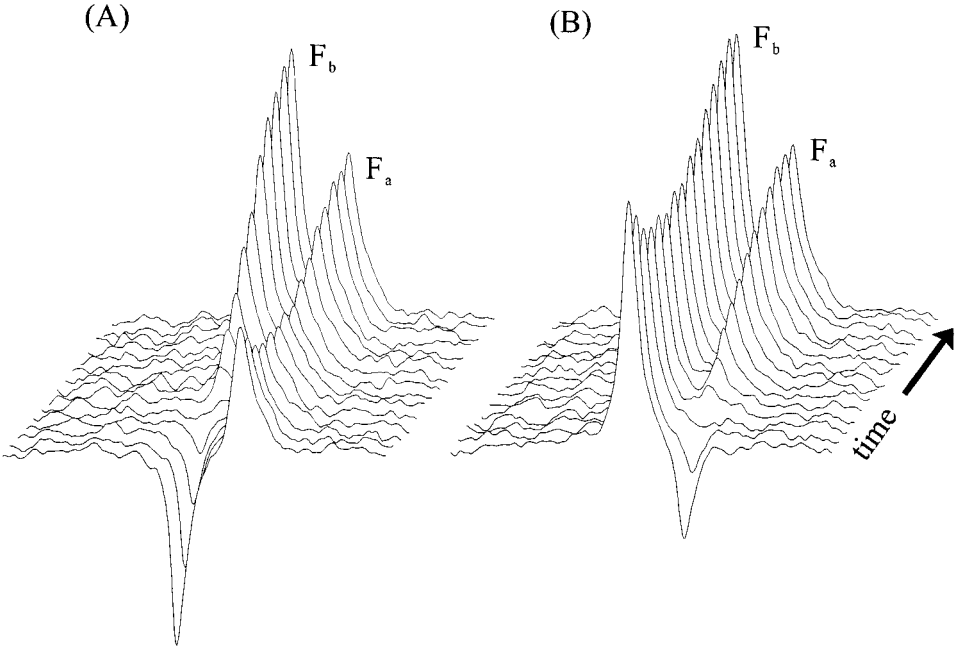

FIGURE 2 SIT-NMR experiments on folded forms at L13(*e*) of GCN4-lzK at 29.7°C. Solvent and peptide chain formality as in Fig. 1. (*A*) F_b resonance initially inverted. (*B*) F_a resonance initially inverted. First spectra are at 0.0 s, last at 1.5 s after Gaussian inversion centered at −0.015 s.

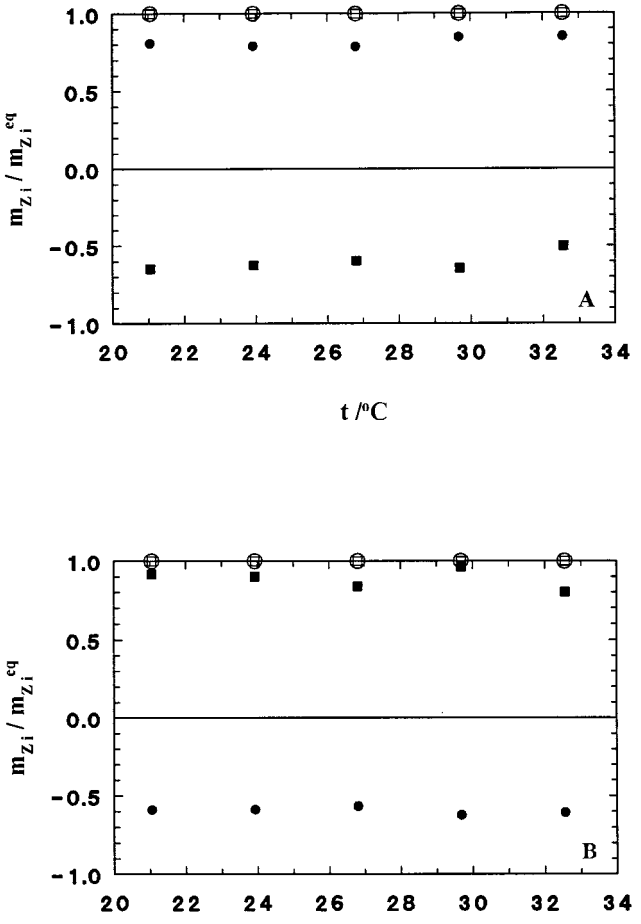

FIGURE 3 Effect of inversion pulse on longitudinal magnetization at L13(*e*) of GCN4-lzK. Solvent and peptide chain formality as in Fig. 1. All magnetizations first normalized to glycine (see text), then self-normalized to equilibrium values (see text). Open symbols, at equilibrium; filled symbols, at 0.0 s after Gaussian inversion centered at −0.015 s. Squares, values at F_a; circles, values at F_b. (*A*) F_a inverted. (*B*) F_b inverted.

and its reciprocal

$$\mathbf{U}^{-1} = \begin{pmatrix} \dfrac{1}{\dfrac{R_a + a_1}{k_{ba}}} & \dfrac{1}{\dfrac{R_a + a_2}{k_{ba}}} \end{pmatrix} \qquad (7b)$$

can be used.

We re-express these equations here, lest the typographical errors that exist in the original references cause confusion. We recognize that our system differs somewhat from those for which this formalism was developed in that F_a and F_b, being dimers, each contain *two* L13(*e*) spins. However, careful re-derivation shows that this has no effect on the equations.

At each temperature the 30 FIDs described above constitute the data base. From it, 12 constants must be extracted: the four rate constants and eight magnetic intensities. The latter comprise the initial ($t = 0$, by definition the time of the first interrogation) and asymptotic ($t \to \infty$) values of both M_{Za} and M_{Zb} after M_{Za} is inverted and the same after M_{Zb} is inverted. The two inversions have the same rate constants, but different boundary conditions.

To obtain the four rate constants, the spin count for each resonance must be determined. We used the Bayes Analysis Package (available from Varian Associates) with procedures that have been described (Bretthorst, 1990, 1990a,b, 1997). The two sets of FIDs were analyzed jointly to determine the number of resonances, their relative spin count, and the frequency, phase, and transverse magnetization decay time constant, T_2^*, of each.

The longitudinal magnetizations of the F_a and F_b resonances at a given temperature provide two distinct time courses for determination of the four rate constants. Additionally, there is prior information about the experiment. For example, the magnetizations return to their equilibrium values, which may be used to eliminate one of the equilibrium magnetizations from the solutions to the differential equations. Also, the physical nature of the rate constants constrains them to be positive quantities within certain wide bounds. Bayesian probability theory was used to incorporate this prior information into the joint analysis of the two time courses. The posterior probability for each of the four rate constants and for each of the four magnetizations in each of the two time courses was computed, conditional on the time course data and the prior information. Probabilities for other quantities (e.g., the ratio of the rate constants) were obtained as well. The computation of the probability distributions employed a Markov chain Monte Carlo integration (Gilks et al., 1996) to produce the required marginal probability density functions.

The samples from the Markov chain were used in a number of ways. Histograms of the samples gave a picture of the output of the Markov chain; the moments were used to generate a maximum entropy representation of the probability density function, and these in turn were plotted and used to curve-fit the histograms; scatter plots of the Markov chain samples were used to diagnose correlations and improve convergence of the simulations; and the mean and mean-squares of the Markov chain provided estimates of the parameters and of their uncertainties.

RESULTS

The $^{13}C^{\alpha}$-NMR spectral basis for this study is shown in Fig. 1. Chemical shifts for L13(*e*) residues in GCN4-lzK lie in the range 55–60 ppm, as established earlier (Lovett et al., 1996; Holtzer et al., 1997) by spectra over the full range of accessible temperatures (8.5–73°C). In the vicinity of room temperature, resonances for two folded forms of L13(*e*) appear: F_a at 58.2 ppm, which predominates at low temperature, and F_b at 58.9 ppm, which predominates at moderate temperature. In the range shown in Fig. 1, very little unfolded population (near 56 ppm) is seen.

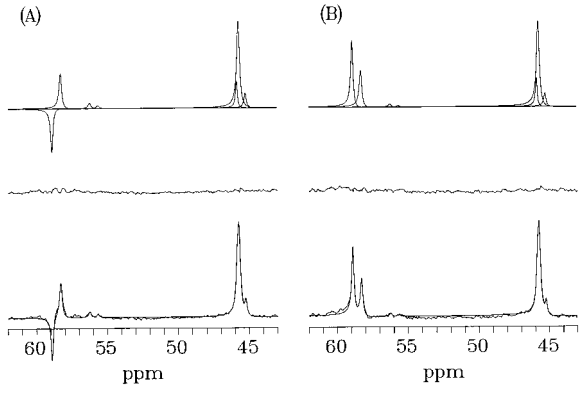

FIGURE 4 Maximum posterior probability fit of $^{13}C^{\alpha}$-NMR spectra at L13(*e*) and G31(*b*) of GCN4-lzK at 29.7°C. Solvent and peptide chain formality as in Fig. 1. In both *A* and *B* the bottom portion shows experimental spectrum (noisy curve) and superposed model spectrum (non-noisy curve); middle portion shows residuals; top portion shows Bayesian spectral decomposition. Inversion is at site F_b via Gaussian pulse at $t = -0.015$ s. (*A*) At $t = 0.0$ s. (*B*) At $t = 1.5$ s.

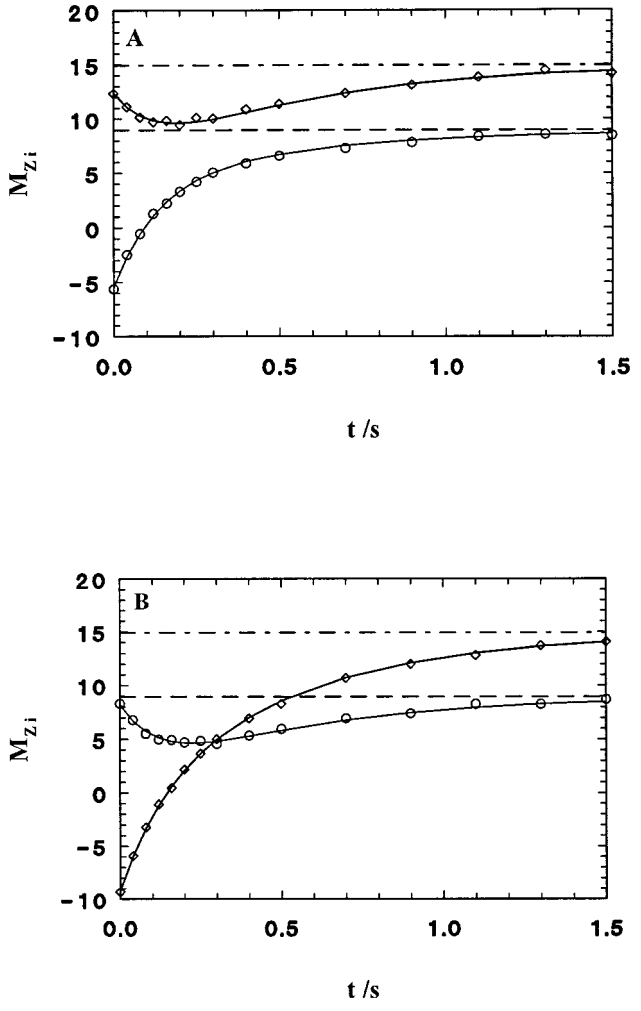

FIGURE 5 Time course of magnetization in SIT experiments for L13(*e*) of GCN4-lzK at 29.7°C. Solvent and peptide chain formality as in Fig. 1. Open circles, experimental F_a magnetizations; open diamonds, experimental F_b magnetizations. Solid curves, solutions to kinetic differential equations with parameters that jointly maximize the posterior probabilities. Dashed horizontal lines, calculated asymptotes for F_a sites. Dot-dashed horizontal lines, calculated asymptotes for F_b sites. (*A*) F_a inverted. (*B*) F_b inverted.

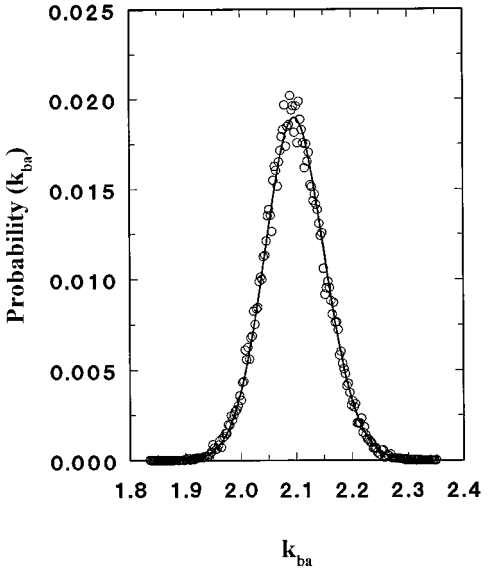

FIGURE 6 Marginal posterior probability distribution for back-reaction rate constant k_{ba} from data of Fig. 5.

In the particular peptide reported on here, G31(*b*) is also labeled. Its resonances appear in the range 44–47 ppm. At this near-C-terminal site a small but significant amount of unfolded form appears upfield (at 45.5 ppm) of the main resonances for folded forms, and two lines (near 45.8 ppm) for folded forms are apparent, although their resolution at G31(*b*) is not nearly as great as at L13(*e*). These glycine resonances will not concern us much here, but they are extremely useful in providing a check on the integrity of the data, since they must remain invariant during the inversions and recoveries of magnetization at L13(*e*).

Fig. 2 shows a typical SIT experiment. The initial inversion of magnetization at F_b (Fig. 2 *A*) is obvious, as is its recovery with time. The effect of inversion at F_b on the resonance at F_a is even more striking. If the two forms were not interconverting on the appropriate time scale, the F_a magnetization would remain unchanged, since that spin system is already at equilibrium. Instead, it first *declines*, as inverted F_b spins change conformation to F_a, then recovers to the equilibrium value. Initial inversion at F_a (Fig. 2 *B*) shows analogous effects.

The performance of the Gaussian inversion pulse may be assessed from Fig. 3, which compares magnetizations just before and just after inversion. To place all the measured longitudinal magnetizations on a comparable basis, they were each divided by the value for glycine (M_{ZG}) in the same spectrum, providing $m_{Za} = M_{Za}/M_{ZG}$ and $m_{Zb} = M_{Zb}/M_{ZG}$. These values were then self-normalized by dividing each by the equilibrium value m_{Zi}^{eq} at the same site. Thus, at spin equilibrium just before inversion, the ordinates at both sites are +1; perfectly frequency-selective inversion would convert the inverted site's value to −1, leaving the

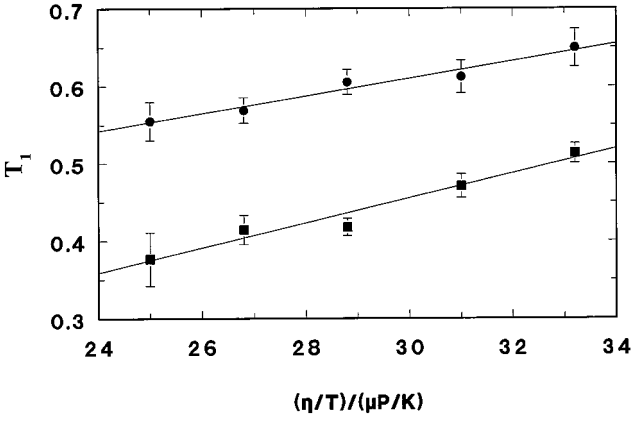

FIGURE 7 SIT-derived spin-lattice relaxation times at site L13(*e*) of GCN4-lzK versus $\eta(T)/T$. Filled squares, F_a; filled circles, F_b. Error bars are from Bayesian probability distributions, as in Fig. 6.

TABLE 1 Thermodynamic and kinetic constants from $^{13}C^{\alpha}$-NMR

Temp. (°C)	T_{1a}*/s	T_{1b}*/s	k_{ab}*/s^{-1}	k_{ba}*/s^{-1}	(k_{ab}/k_{ba})*	$K_{eq}^{\#}$
21.1	0.513 ± 0.013	0.649 ± 0.024	0.818 ± 0.027	1.052 ± 0.035	0.778 ± 0.008	0.770
23.9	0.471 ± 0.015	0.612 ± 0.021	1.358 ± 0.041	1.341 ± 0.041	1.012 ± 0.009	1.017
26.8	0.418 ± 0.011	0.605 ± 0.016	2.180 ± 0.046	1.605 ± 0.034	1.358 ± 0.010	1.301
29.7	0.414 ± 0.019	0.569 ± 0.017	3.496 ± 0.088	2.098 ± 0.055	1.666 ± 0.017	1.737
32.6	0.377 ± 0.035	0.555 ± 0.025	5.896 ± 0.279	2.605 ± 0.125	2.264 ± 0.037	1.968

Values for $F_a \rightleftarrows F_b$ at position L13(e) of GCN4-lzK in $(NaCl)_{100}(NaPi)_{50}(D_2O)_{5514}$(7.4).
*From SIT.
#From equilibrium magnetization intensities.

uninverted site unchanged at +1. As seen in Fig. 3 *A*, inversion at F_a is substantial but not complete; the ordinate goes from +1 to ~−0.6, a change essentially independent of temperature.

In the same experiment (Fig. 3 *A*), the F_b resonance is not quite independent of the inversion at F_a, the ordinate at F_b changing from +1 to +0.8, again independent of temperature. This picture changes only slightly when the initial inversion is at F_b (Fig. 3 *B*). There, the ordinate also changes from +1 to −0.6, but even less of the inversion bleeds over to F_a, where it changes from +1 to +0.9.

The inversion protocol thus provides ample dynamic range for characterization of the magnetization recovery. Our data analysis makes no assumptions concerning the initial inversions, so there is no impediment to obtaining reliable values. The quality of the Bayesian analysis may be judged from Fig. 4, the lower positions of which show the first (0.0 s, Fig. 4 *A*) and last (1.5 s, Fig. 4 *B*) spectra taken after Gaussian inversion (centered at $t = -0.015$ s) of F_b. In each case, the experimental spectrum (*noisy solid curve*) is overlaid with the Bayesian result (*non-noisy solid curve*). The residuals (*middle graph*) indicate quite satisfactory agreement. The individual contributing resonances found by the Bayesian analysis software are delineated in the upper parts of Fig. 4.

Sample plots of the time course of recovery of the resulting magnetization intensities are shown in Fig. 5 for inversion at each site at 29.7°C. Fig. 5 illustrates how well the two experimental time courses are modelled by Bayesian probability theory, using the solutions to the kinetic differential equations with values of the parameters that jointly maximize the posterior probability. Fig. 6 gives a sample Bayesian probability plot for the rate constant k_{ba} at 29.7°C. The most probable values and error estimates are available from such fits.

The marginal posterior probabilities for the intrinsic spin-lattice relaxation times, T_{1a} and T_{1b}, are obtained from the Markov simulations. These relaxation times depend upon the molecular rotational correlation times, which are directly proportional to the medium's viscosity (η, which is temperature-dependent) and inversely proportional to the Kelvin temperature. Fig. 7 shows these T_{1i} values, plotted

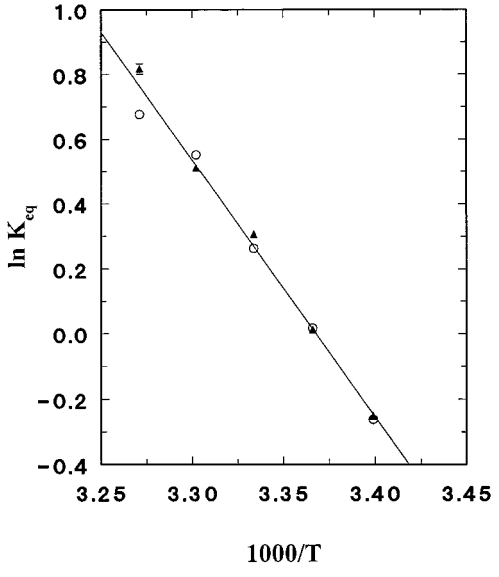

FIGURE 8 van't Hoff plot of equilibrium constants at site L13(e) of GCN4-lzK. Open circles, $[F_b]/[F_a]$ at spin equilibrium; filled triangles, k_{ab}/k_{ba} from SIT; solid line, least-squares fit. Error bars appear only where error is larger than the symbol. Derived thermodynamic quantities are in Table 2.

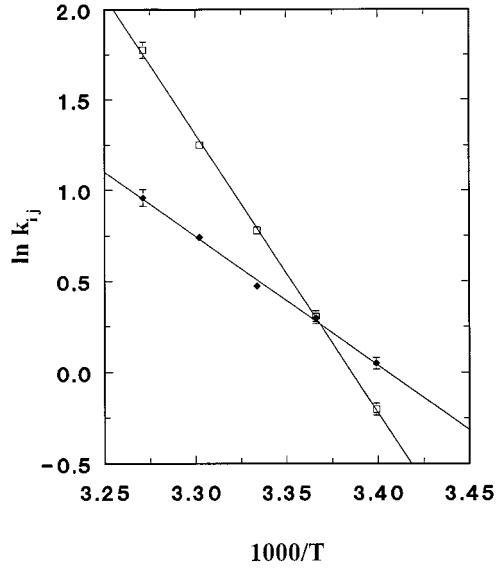

FIGURE 9 Arrhenius plots of rate constants for interconversion of folded forms at site L13(e) of GCN4-lzK. Open squares, k_{ab}; filled diamonds, k_{ba}; solid lines, least-squares fits to Eyring equation. Error bars appear only where error is larger than the symbol. Derived kinetic quantities are in Table 2.

TABLE 2 Derived thermodynamic and kinetic parameters

ΔG° *	ΔH° #	ΔS° §	$\Delta G^{\ddagger}_{ab,ba}$*	$\Delta H^{\ddagger}_{ab}$ #	$\Delta S^{\ddagger}_{ab}$ §	$\Delta H^{\ddagger}_{ba}$ #	$\Delta S^{\ddagger}_{ba}$ §
0.00 ± 0.02	15.7 ± 0.6	52.8 ± 1.9	17.20 ± 0.01	29.8 ± 0.4	42.2 ± 1.4	13.5 ± 0.5	−12.7 ± 1.5

For $F_a \rightleftarrows F_b$ at position L13(*e*) of GCN4-lzK in $(NaCl)_{100}(NaPi)_{50}(D_2O)_{5514}$(7.4).
*kcal/mol; interpolated to 24°C using van't Hoff (ΔG°) or Eyring ($\Delta G^{\ddagger}$) equation; error estimates from r.m.s. residuals in Figs. 8 or 9.
#kcal/mol; error estimates from standard least-squares analysis.
§cal/(K · mol); error estimates from standard least-squares analysis.

versus η/T. The positive slope of these plots is expected for a molecule of the size of GCN4-lzK, whose rotational relaxation time is likely appreciable. The numerical values of these spin-lattice relaxation times and of the other kinetic and thermodynamic constants are summarized in Table 1.

Fig. 8 shows the relevant values from Table 1 as a van't Hoff plot. The equilibrium constants for the conformational change as determined from data at spin equilibrium (*open circles*) agree well with those determined as the ratio of the rate constants (k_{ab}/k_{ba}, *filled triangles*) from dynamic SIT, and both are well fit by the van't Hoff equation (*solid line*) with constant enthalpy. Likewise, in Fig. 9, the Arrhenius plots of the rate constants k_{ab} (*open squares*) and k_{ba} (*filled diamonds*) are well fit by the Eyring equation (*solid lines*). Thermodynamic and kinetic parameters derived from these data are given in Table 2.

DISCUSSION

Earlier work showing site-dependent thermal unfolding curves for GCN4-lzK leaves little doubt that the equilibrium population of conformational states is not of the simple two-state sort (Holtzer et al., 1997). The appearance of NMR lines for more than one folded form at many sites is further evidence of this complexity (Lovett et al., 1996). The data presented above represent a first step in characterizing the equilibrium and kinetic features of the interconversion of such locally folded forms.

In particular, Tables 1 and 2 provide information on the transition between the ensemble of coiled coils in folded form F_a and the ensemble in folded form F_b at position L13(*e*). The energetic parameters determined are schematically displayed in Fig. 10. For all three of the state functions shown, the value for F_a is arbitrarily set to zero.

In Fig. 10 the temperature 24°C is selected because it is the center of the transition region where the standard Gibbs energy change is zero, making the populations of F_a and F_b equal. The observed overall standard enthalpy change of the transition, 15.7 kcal/mol, is quite substantial, indicating markedly higher energy for F_b compared with F_a. However, at this temperature it is precisely compensated by F_b's substantially higher entropy. Both values suggest that F_b is more loosely folded than F_a.

As seen in Fig. 10, the Gibbs energies of activation for the forward and reverse transitions are also substantial, ~17 kcal/mol, which slows interconversion and is responsible for our fortuitous ability to observe separate NMR resonance lines for F_a and F_b. Even more remarkable is the activation enthalpy for the $F_a \rightarrow F_b$ direction, which is ~30 kcal/mol. The enthalpy of *total* unfolding for GCN4-lzK is not yet known, but the values for related peptides suggest that it is ~45–60 kcal/mol (Kenar et al., 1995). Thus, the activation enthalpy for the forward transition between our two folded forms is a substantial fraction of the total unfolding enthalpy. The overall transition enthalpy and the activation enthalpy for the reverse process, 15.7 and 13.5 kcal/mol respectively, are smaller, but also substantial.

By themselves, these findings concerning the magnitudes of the activation enthalpies suggest that the transition ensemble of states involves a considerable degree of unfolding at position L13(*e*). However, the entropic contribution to the Gibbs energy of activation shows that the case is not so simple. An appreciably unfolded transition state would be expected to have an entropy considerably higher than that of either folded form. In contrast, Fig. 10 shows that its entropy is in-between, being considerably greater than F_a's but slightly *less* than F_b's. It seems, then, that this transition ensemble is either not substantially unfolded or localizes a rather large amount of solvent.

The precise nature of the structural differences between the two folded forms is not yet known, nor can we precisely specify the structural features of the transition state. It will likely take some combination of multidimensional NMR-structural studies and theoretical simulations to answer the former question, whereupon dynamic simulations may shed some light on the latter one. The characterization of the energetics reported here provides constraints that answers from such future studies must satisfy.

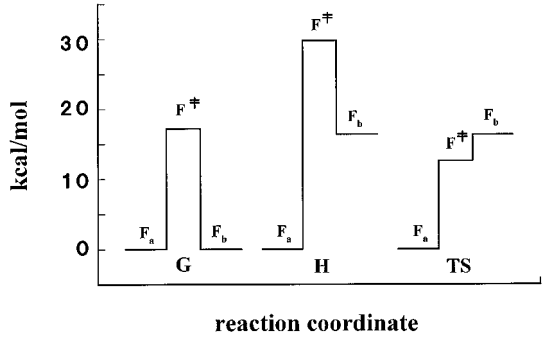

FIGURE 10 Schematic energy diagram at interpolated midpoint (24°C) of reaction $F_a \rightleftarrows F_b$. Double-dagger superscript designates transition state. From left to right, standard Gibbs energy, enthalpy, and temperature-entropy product. Abscissas (reaction coordinate) are shifted to allow parallel presentation. Ordinates (G, H, and TS) for form F_a are arbitrarily set to zero.

More insight into the many remaining questions may be forthcoming from similar SIT studies of the interconversion of folded forms at sites other than L13(*e*). Moreover, our preliminary studies indicate the feasibility, in a somewhat higher temperature range, of examining the interconversion of F_b with the *unfolded* form at specific sites by the same SIT technique.

Mass spectrometry was provided by the Washington University Mass Spectrometry Resource, a National Institutes of Health Research Resource (Grant P41RR0954). Synthesis of the peptide was carried out by Dr. Eva Lovett. Development of the Bayesian techniques employed here was supported by National Institutes of Health Grant NS-35912 and by a license agreement with Varian Associates. One of us (A.H.) acknowledges the aid of the Luftmensch Society.

REFERENCES

Bretthorst, G. L. 1990. Bayesian analysis. I. Parameter estimation using quadrature NMR models. *J. Magn. Reson.* 88:533–551.

Bretthorst, G. L. 1990a. Bayesian analysis. II. Model selection. *J. Magn. Reson.* 88:552–570.

Bretthorst, G. L. 1990b. Bayesian analysis. III. Applications to NMR signal detection, model selection, and parameter estimation. *J. Magn. Reson.* 88:571–595.

Bretthorst, G. L. 1997. Bayesian Analysis Software Package User Guide. Pub. No. 87–190172-00. Rev. A0197, Varian Associates, Inc., Palo Alto, CA.

Gilks, W. R., S. Richardson, and D. J. Spiegelhalter. 1996. Markov Chain Monte Carlo in Practice. Chapman & Hall, London.

Goodman, E. M., and P. S. Kim. 1991. Periodicity of amide proton exchange rates in a coiled-coil leucine zipper peptide. *Biochemistry*. 30:11615–11620.

Holtzer, M. E., D. L. Crimmins, and A. Holtzer. 1995. Structural stability of short subsequences of the tropomyosin chain. *Biopolymers.* 35: 125–136.

Holtzer, A., M. E. Holtzer, and J. Skolnick. 1990. Does the unfolding transition of two-chain, coiled-coil proteins involve a continuum of intermediates? *In* Protein Folding. L. M. Gierasch and J. King, editors. AAAS Books, Washington, D.C. 177–190.

Holtzer, M. E., E. G. Lovett, D. A. d'Avignon, and A. Holtzer. 1997. Thermal unfolding in a GCN4-like leucine zipper: $^{13}C^{\alpha}$-NMR chemical shifts and local unfolding equilibria. *Biophys. J.* 73:1031–1041.

Kenar, K. T., B. Garcia-Moreno, and E. Freire. 1995. A calorimetric characterization of the salt dependence of the stability of the GCN4 leucine zipper. *Protein Sci.* 4:1934–1938.

Lovett, E. G., D. A. d'Avignon, M. E. Holtzer, E. H. Braswell, D. Zhu, and A. Holtzer. 1996. Observation via one-dimensional $^{13}C^{\alpha}$ NMR of local conformational substates in thermal unfolding equilibria of a synthetic analog of the GCN4 leucine zipper. *Proc. Natl. Acad. Sci. USA*. 93: 1781–1785.

Lupas, A. 1996. Coiled coils: new structures and new functions. *TIBS*. 21:375–382.

McConnell, H. M. 1958. Reaction rates by nuclear magnetic resonance. *J. Chem. Phys.* 28:430–431.

McLachlan, A. D., and M. Stewart. 1975. Tropomyosin coiled-coil interactions. Evidence for an unstaggered structure. *J. Mol. Biol.* 98:293–304.

O'Shea, E. K., J. D. Klemm, P. S. Kim, and T. Alber. 1991. X-ray structure of the GCN4 leucine zipper, a two-stranded, parallel coiled coil. *Science*. 254:539–544.

O'Shea, E. K., R. Rutkowski, and P. S. Kim. 1989. Evidence that the leucine zipper is a coiled coil. *Science*. 243:538–542.

Privalov, P. L. 1982. Stability of proteins: proteins which do not present a single cooperative system. *Adv. Protein Chem.* 35:1–104.

Rudin, M., and A. Sauter. 1992. Measurement of reaction rates in vivo using magnetization transfer techniques. *In* NMR Basic Principles and Progress, P. Diehl, E. Fluck, H. Günther, R. Kosfeld, and J. Seelig, editors. 27:257–293.